Research Article

Jianfei Qin, Lifen Tong*, Liang He, Xiaobo Liu, and Xiran Tang*

Lightweight and high-strength polyarylene ether nitrile-based composites for efficient electromagnetic interference shielding

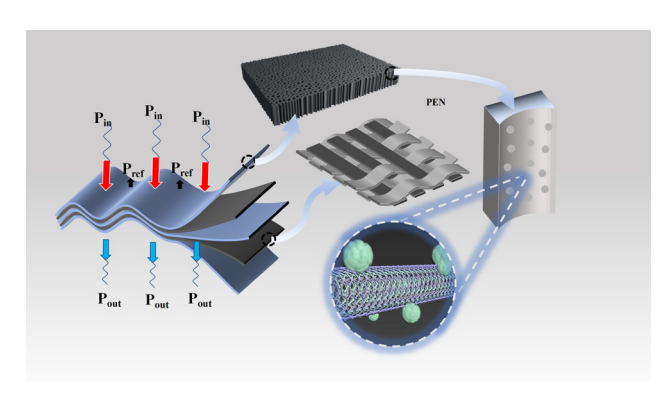
https://doi.org/10.1515/ntrev-2023-0167 received September 18, 2023; accepted November 14, 2023

Abstract: The proliferation of electronic devices and the widespread adoption of microwave-based technologies have resulted in a notable rise in electromagnetic radiation pollution. In present work, a novel flexible lightweight polyarylene ether nitrile (PEN)-based composite for efficient electromagnetic interference (EMI) shielding was prepared by introducing dual-loss hybrid material (PKMWCNT@Fe₃O₄) into PEN via non-solvent induce phase separation method and assembling it layer-by-layer with carbon fiber (CF) fabric. The porous morphology of the PEN layer, the electrical conductivity of the CF fabric, and the dual-loss property of the filler enable the material to reflect and absorb electromagnetic waves multiple times, resulting in superior electromagnetic shielding performance. With the addition of PKMWCNT@Fe₃O₄ at a mass fraction of 50%, the EMI SE_T and specific shielding effectiveness SSE/t can reach up to 47.08 dB and 617 dB cm²/g, respectively, indicating absorption dominated shielding mechanism. Furthermore, the material exhibits a lightweight nature with a density of 0.55 g/cm³, and excellent mechanical properties, including

Novel CN Polymeric Materials, Chengdu, 610054, China,

e-mail: tonglifen0214@uestc.edu.cn

Jianfei Qin: Yangtze Delta Region Institute (Huzhou), University of Electronic Science and Technology of China, Huzhou, 313001, China Liang He, Xiaobo Liu: School of Materials and Energy, University of Electronic Science and Technology of China, Chengdu, 610054, China; Sichuan Province Engineering Technology Research Center of Novel CN Polymeric Materials, Chengdu, 610054, China



Graphical abstract

a tensile strength of 43.98 MPa and elongation at break of 43.32%. This work presents a new approach to prepare high-performance composites that are both lightweight and resistant to secondary contamination by electromagnetic waves.

Keywords: dual-loss filler, MWCNT, carbon fiber fabric, electromagnetic properties

1 Introduction

Electromagnetic shielding functional materials play a vital role in addressing the issue of electromagnetic wave pollution in both military and civilian sectors [1–4]. As electronic devices and telecommunication systems continue to advance rapidly, electromagnetic interference (EMI) has become increasingly significant [5,6]. To mitigate the harmful effects of EMI, various shielding techniques have been developed, among which electromagnetic shielding materials offer an effective solution [7,8]. These materials are designed to attenuate or redirect electromagnetic waves, preventing them from interfering with nearby electronic devices. They have extensive applications in industries such as aerospace, telecommunications, automotive, and medical, where the reliable operation of electronic equipment is of utmost importance [9–11].

^{*} Corresponding author: Lifen Tong, Yangtze Delta Region Institute (Huzhou), University of Electronic Science and Technology of China, Huzhou, 313001, China; School of Materials and Energy, University of Electronic Science and Technology of China, Chengdu, 610054, China; Sichuan Province Engineering Technology Research Center of

^{*} Corresponding author: Xiran Tang, School of Materials and Energy, University of Electronic Science and Technology of China, Chengdu, 610054, China; Sichuan Province Engineering Technology Research Center of Novel CN Polymeric Materials, Chengdu, 610054, China, e-mail: xirant@163.com

Electromagnetic shielding materials can be categorized based on their shielding mechanisms, including reflective shielding materials, absorptive shielding materials, scattering shielding materials, and multilayer composite shielding materials. Reflective shielding materials are conductive materials that achieve shielding by reflecting electromagnetic waves [12,13]. When electromagnetic waves interact with these materials, the free electrons within the material are excited by the electromagnetic field, generating opposing currents to counteract the energy of the incident waves [14,15]. Absorptive shielding materials absorb electromagnetic waves by converting their energy into other forms [16–19]. These materials typically have good electromagnetic wave absorption capabilities, such as high dielectric loss or conversion of electromagnetic waves into heat energy [20-23]. Scattering shielding materials utilize their unique structures and shapes to cause multiple reflections and scattering of electromagnetic waves on the material surface, achieving shielding through interference effects [24,25]. Multilayer composite shielding materials consist of a combination of different types of shielding materials in a layered structure [26-28]. By designing different layers of material combinations, multiple mechanisms such as reflection, absorption, and scattering can be utilized to achieve better shielding effects [29,30].

Traditional metals and their alloys have limitations in electromagnetic shielding due to factors such as high weight, high cost, and poor corrosion resistance [31,32]. Therefore, polymer-based or carbon-based electromagnetic shielding materials are receiving increasing academic attention [33-37]. Gao et al. presented a comprehensive review on graphene-based materials for electromagnetic shielding applications [24]. The authors discuss various design strategies at different scales, ranging from molecular to macroscopic levels, aiming to enhance the electromagnetic shielding performance of graphene-based materials. These design strategies encompass the incorporation of graphene at the molecular scale, the utilization of micro/nanostructures, the development of macrostructures, and the integration of design approaches for multiscale assemblies. Kong et al. conducted a study on the development of an electromagnetic shielding shape memory polyimide material [38]. In their research, they synthesized the material by incorporating 5% short carbon fibers (CFs) and 4% carbon black into a shape memory polyimide matrix. As a result, this composite material achieved an impressive average EMI shielding effect of 23.9 dB in the X-band, despite having a relatively thin thickness of 0.35 mm. Zhang et al. successfully fabricated flexible composite films comprising Ti₃C₂T_x nanosheets embedded in an aramid nanofiber/polyvinyl alcohol (PVA) matrix [39]. This composite material exhibited an exceptional EMI shielding effectiveness of 70 dB, highlighting its remarkable capability to attenuate and block electromagnetic radiation. Zheng *et al.* innovatively created a lightweight polyurethane (PU) composite foam designed specifically for EMI shielding purposes [40]. Fe $_3$ O $_4$ @PVA and graphene oxide@silver were incorporated into a PU matrix, which facilitated the formation of an excellent network structure within the PU foam skeleton. This enhanced network structure significantly contributed to the overall EMI shielding effectiveness and mechanical performance of the composite foams.

Polyarylene ether nitrile (PEN) is a leading special engineering plastic that finds extensive applications in both civil and military sectors due to its favorable characteristics, including exceptional high-temperature resistance. impressive strength, elevated modulus, and remarkable corrosion resistance, etc. [41-46]. In view of the excellent properties and processability of polyarylether nitrile, researchers have developed a series of functional composites. In view of the excellent properties and processability of PEN, researchers have developed a series of functional composites. Wang et al. fabricated an anti-bacterial robust Ag@PDA/PEN electrospinning nanofibrous membrane for oil-water separation by combining PEN with polydopamine (PDA) and Ag nanoparticles (NPs) [47]. He et al. prepared high-performance thermally conductive composites by introducing boron nitride nanosheets and benzocyclobutene into PEN [48]. In the present work, PEN is used as a carrier for electromagnetic shielding fillers, and a novel electric/magnetic dual-loss nanomaterials of multi-walled carbon nanotubes (MWCNT)@Fe₃O₄ hybrid material and CF are used as functional fillers. First, the MWCNT@Fe₃O₄ hybrid material was prepared using a coprecipitation method, which effectively suppresses the reflection of electromagnetic waves, thus enhancing the reliability and durability of the shielding system. Subsequently, the MWCNT@Fe₃O₄ hybrid material was introduced into PEN matrix, and assembled with CF fabric laver-by-laver, Lastly, the composites of PEN/MWCNT@Fe₃O₄/CF fabric were prepared with non-solvent induced phase separation method. The influence of different filler contents on structural morphology and comprehensive properties was studied, and the shielding mechanism of the PEN/MWCNT@Fe₃O₄/CF fabric composites was investigated, which will provide reference for the suitable designs of multifunctional PEN/CF fabric composites with adjustable structure and properties and provide a theoretical basis for the realization of a more efficient shielding effectiveness for the next-generation new composites.

2 Experimental

2.1 Materials

PEN was synthesized from our labs [42]. The carboxylated carbon nanotubes (MWCNT-COOH), dopamine hydrochloride,

tris (hydroxy) aminomethane, N,N-dimethylacetamide (DMAc), FeCl₂·4H₂O, FeCl₃·6H₂O, NH₃·H₂O, KH550, glycerol, and anhydrous ethanol were purchased from Chengdu Kelong Chemical Reagents Co., Ltd (Chengdu China). The CF fabric used in the study was obtained from Yixing Zhongfu Carbon Fiber Products Co.

2.2 Preparation of PEN/CF electromagnetic shielding composites

2.2.1 Synthesis of PKMWCNT@Fe₃O₄ hybrid nanomaterials

PKMWCNT@Fe₃O₄ hybrid nanomaterials were synthesized as shown in Figure 1(a). First, dissolve FeCl₂·4H₂O (0.373 g) and FeCl₃·6H₂O (1.014 g) into 300 mL deionized water under the protection of N₂ to form a homogeneous solution. Then, carboxylated carbon nanotubes (MWCNT-COOH, 0.3 g) was added under mechanical stirring at 300 rpm with ultrasonic treatment. After MWCNT-COOH was completely dispersed in the solution, the water bath was warmed up to 80°C and ammonia was added drop by drop until pH = 11. After reaction for 2 h, the MWCNT@Fe₃O₄ hybrid filler was collected with magnet, washed repeatedly with deionized water, and then freeze-dried for 48 h to obtain MWCNT@Fe₃O₄. Next, MWCNT@Fe₃O₄ (0.1 g), dopamine (DA, 40 mg), and KH550 (8 mg) were dispersed in 100 mL deionized water and adjusted the solution with Tris until pH = 8.5. The reaction was reacted at 300 rpm for 8 h under mechanical agitation and sonicated at room temperature. After completion of the reaction, these functionalized fillers were separated in a centrifuge, and were freeze-dried for 48 h after several washes and named as PKMWCNT@Fe₃O₄.

2.2.2 Preparation of PEN/PKMWCNT@Fe₃O₄/CF composites

The preparation process of PEN/PKMWCNT@Fe₃O₄/CF composites is shown in Figure 1(b). About 0.18 g of PEN, 0.005 g of glycerol, and 1.8 ml of DMAc were mechanically stirred at 300 rpm for 5 h until completely dissolved and a homogeneous solution was formed, and then left to stand for 5 h to completely eliminate the air bubbles, and is named as solution A. Meanwhile, PKMWCNT@Fe₃O₄ nanomaterials were dispersed into 10 mL DMAc to form a homogeneous solution B with mechanical stirring at 300 rpm and ultrasonic treatment, and the concentrations were 0, 12.5, 25, and 50 wt%, respectively. Solution B was then mixed with solution A for 5 h to form solution C. Pour an appropriate amount of the

above solution onto a flat and clean glass plate and use a wet film preparation apparatus to push out a 600 µm liquid film, followed by placing a washed 1 cm × 1 cm square CF fabric lightly on it and pouring an appropriate amount of solution to push out the liquid film again, changing the amount of CF fabric and solution according to actual needs. The glass plate and the liquid/solid multi-phase mixture were immersed in a deionized water coagulation bath. The sample fell off from the glass plate by themselves. Then it was continued to be immersed in deionized water for 24 h to displace solvents and obtain the wet state PEN/PKMWCNT@Fe3O4/CF complex. The above obtained wet state complexes were dried at 60°C for 24 h to obtain PEN/MWCNT@Fe₃O₄/CF composites. The samples were named as $P_{mPKCFx}C_n$, where m and n represent the number of layers of PEN and CF, respectively, PKCF represents PKMWCNT@Fe₃O₄ and x represents the mass percentage of PKMWCNT@Fe₃O₄ in the PEN layer.

2.3 Characterization

The structure of filler was characterized by infrared spectroscopy (Fourier transform infrared [FTIR]) using a Shimadzu 8400S infrared spectrometer with a wavelength of 4,000-400 cm⁻¹. Field emission scanning electron microscopy (FE-SEM; Hitachi SU8010) was employed to characterize the microscopic morphology of the dual-loss filler and PEN/PKMWCNT@Fe₃O₄/CF composites. The EMI shielding effectiveness (SE) of the multilayered films was evaluated in the X-band frequency range of 8.2–12.4 GHz using a Keysight PNA Network Analyzer N5224B, which operated based on the coaxial method. By analyzing the scattering parameters (S11 and S21) obtained directly from the vector network analyzer, it was possible to calculate various EMI shielding parameters. Specifically, the power coefficients of reflectivity (R), transmissivity (T), and absorptivity (A) were calculated from the scattering parameters. Based on these values, the total EMI shielding effectiveness (SE_T), reflection (SE_R), absorption (SE_A) , and multiple reflections (SE_M) were determined using the relevant equations [49]:

$$R = |S_{11}|^2, (1)$$

$$T = |S_{21}|^2, (2)$$

$$A = 1 - (T + R), \tag{3}$$

$$SE_T = 10\log(1/T), \tag{4}$$

$$SE_R = 10 \log(1/1 - R),$$
 (5)

$$SE_A = 10 \log[(1 - R)/T],$$
 (6)

$$SE_T = SE_R + SE_A + SE_M. (7)$$

4 — Jianfei Qin et al. DE GRUYTER

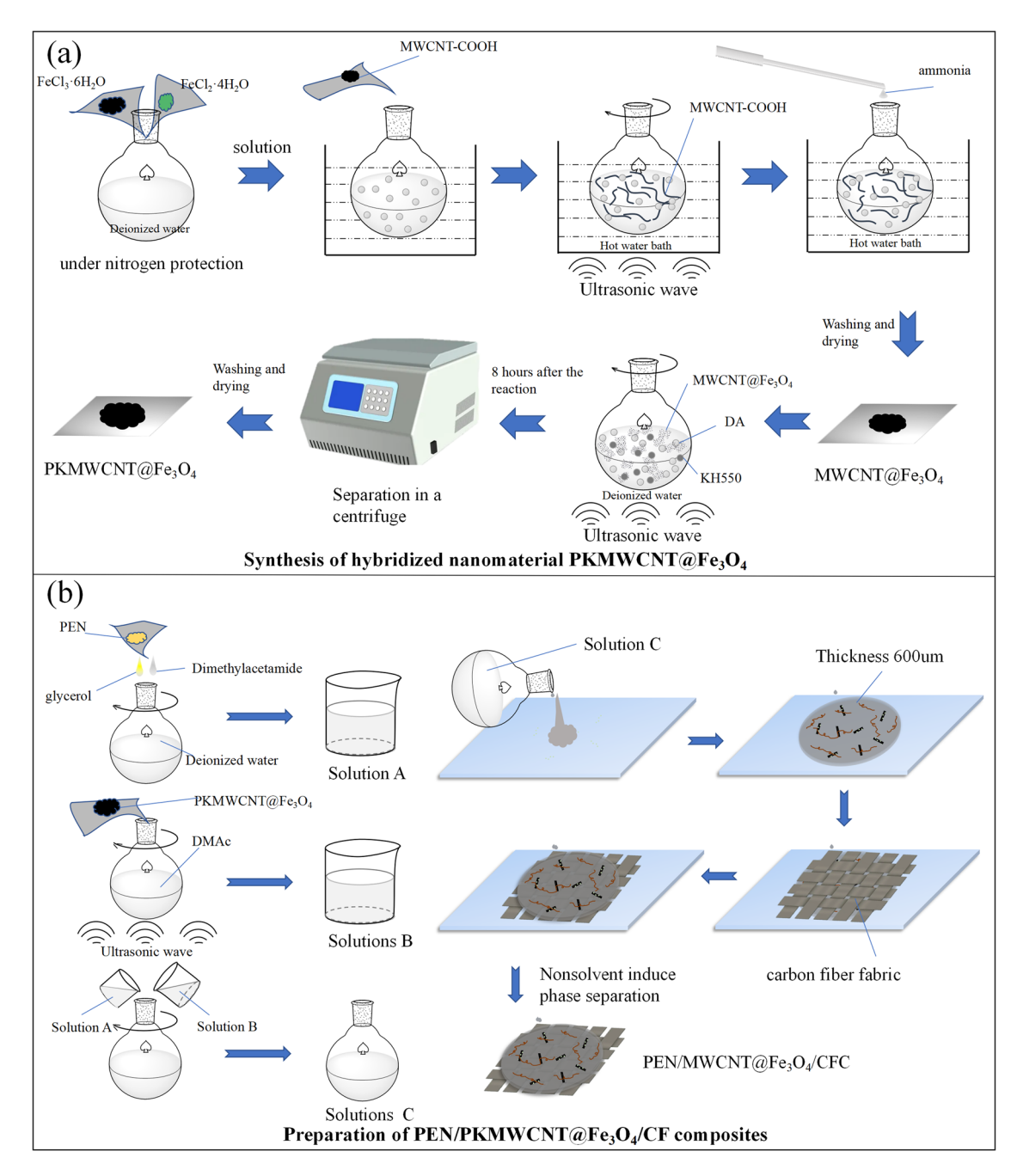


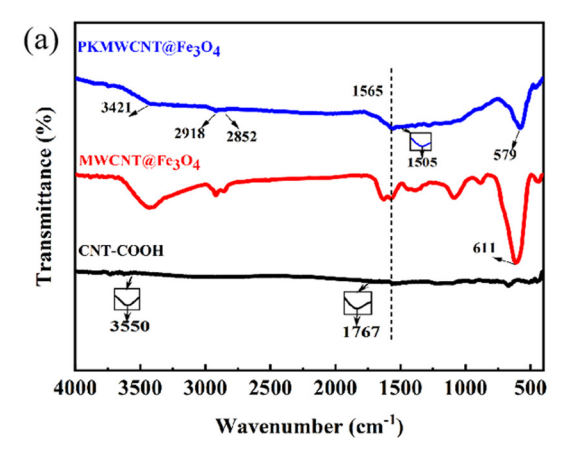
Figure 1: Preparation of (a) hybridized nanomaterial PKMWCNT@Fe₃O₄ and (b) PEN/PKMWCNT@Fe₃O₄/CF composites.

Typically, the contribution of SE_M can be disregarded when the SE_T is equal to or greater than 15 dB [50]. The conductivity of composites was measured on a four-point probe resistivity determiner (RTS-8). The magnetic properties of the samples were evaluated using a vibrating sample magnetometer from Riken Denshi (BHV-525, USA). The mechanical properties of all samples were tested by a universal testing machine with a crosshead speed of 1 mm/min. Thermogravimetric analysis was performed on a TA-Q50 in a nitrogen atmosphere with a ramp rate of 20° C/min.

3 Results and discussion

3.1 PKMWCNT@Fe₃O₄ hybrids materials

The successful preparation of the hybrid CNT is verified using FTIR analysis. In Figure 2(a), all curves have a small peak at 1,565 cm⁻¹, corresponding to the carbon skeleton of the carbon nanotubes [51]. Curve (a) shows a faint peak at 3,550 cm⁻¹, which corresponds to the -OH of the carboxylate group on the MWCNT-COOH [52], and the small peak at



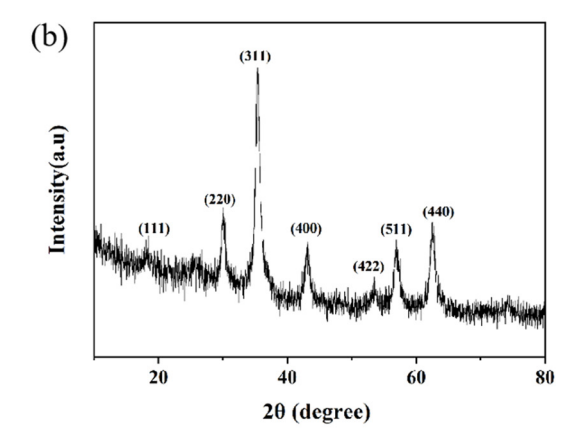


Figure 2: (a) FTIR curves of MWCNT-COOH, MWCNT@Fe₃O₄, and PKMWCNT@Fe₃O₄. (b) XRD pattern of PKMWCNT@Fe₃O₄.

1,767 cm⁻¹ corresponds to C=0. Curve (b) displays a distinct absorption peak at 611 cm⁻¹, which represents the stretching vibration peak of Fe-O in Fe₃O₄ [53]. Curve (c) corresponds to the PKMWCNT@Fe₃O₄ nanomaterials, where the broad peak at 3,421 cm⁻¹ corresponds to the stretching vibration of -OH and -NH-, and the absorption peak at 1,505 cm⁻¹ corresponds to the bending vibration of -NH-. The characteristic peaks at 2,918 and 2,852 cm⁻¹ correspond to the asymmetric stretching vibration and symmetric stretching vibration of methylene, respectively [54]. Based on these results, it is reasonable to infer that PKMWCNT@Fe₃O₄ and cross-linked core-shell structure PKMWCNT@ Fe₃O₄ nanohybrid materials have been successfully prepared. Figure 2(b) shows the XRD pattern of PKMWCNT@ Fe₃O₄. The diffraction peaks at $2\theta = 18.7^{\circ}$, 30.3°, 35.8°, 43.4°, 53.8°, 57.2°, and 63.0° are attributed to (111), (220), (311), (400), (422), (511), and (440) (JCPDS No. 19-0629) crystal planes of spinel Fe₃O₄.

The SEM images demonstrate the microscopic morphology of the hybridized particles. Specifically, Figure 3(a)–(c) shows the morphologies of pristine MWCNT-COOH,

MWCNT@Fe₃O₄, and PKMWCNT@Fe₃O₄, respectively, at a magnification of 160,000. From Figure 3(b), it is evident that carbon nanotubes are grown with nearly spherical particles, which is precisely Fe₃O₄ microspheres grown *in situ* on active sites of carbon tubes, and these microspheres have diameters ranging from 30 to 50 nm. Also, Figure 3(c) shows the microscopic morphology of the PKMWCNT@Fe₃O₄, and it can be seen that the spherical particles on these carbon nanotubes are slightly fuller and the surface is also slightly rougher compared to MWCNT@Fe₃O₄. This difference is attributed to the cross-linking reaction between DA and KH550 on the surface of MWCNTs, leading to the wrapping of PKMWCNT@Fe₃O₄. Hence, the SEM results can further demonstrate the successful preparation of hybrid PKMWCNTs fillers.

Figure 4 is the hysteresis loops of hybrid materials. It can be seen that both are typical soft magnetic materials. The saturation magnetization intensity (Ms) of the MWCNT@Fe $_3$ O $_4$ nanomaterial is higher than that of the PKMWCNT@Fe $_3$ O $_4$. The Ms of former is 34.03 emu/g, while the latter is 24.80 emu/g. Since dopamine hydrochloride and KH550 cross-link on the surface of magnetic carbon nanotubes

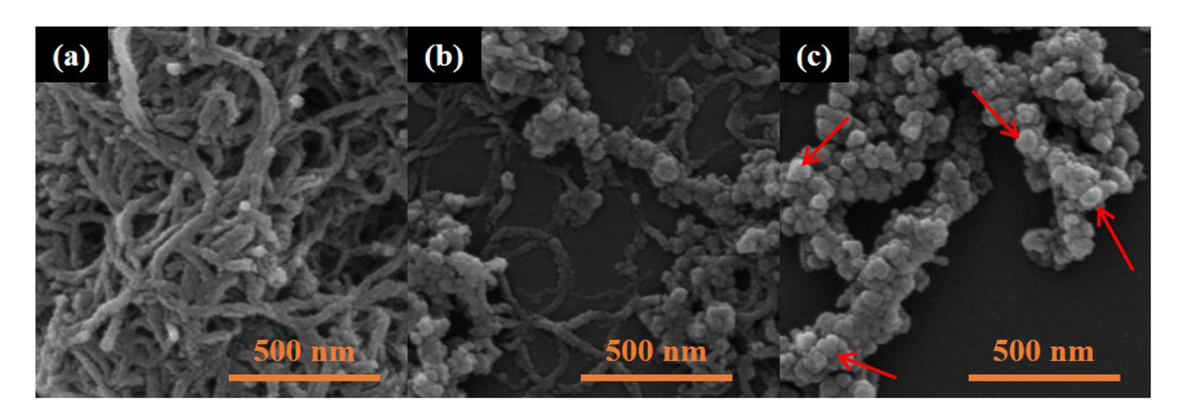


Figure 3: SEM images of (a) MWCNT-COOH, (b) MWCNT@Fe₃O₄, and (c) PKMWCNT@Fe₃O₄.

6 — Jianfei Qin et al. DE GRUYTER

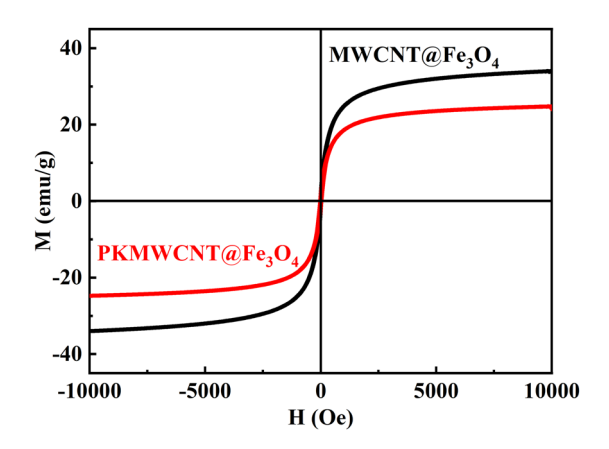


Figure 4: Hysteresis loops of MWCNT@Fe₃O₄ and PKMWCNT@Fe₃O₄.

to form a polymer shell, the mass share of Fe_3O_4 in the whole PKMWCNT@ Fe_3O_4 is reduced.

3.2 PEN/PKMWCNT@Fe₃O₄/CF composites

The chemical structure of $P4_{PKCFx}C3$ composites is investigated using FTIR. As depicted in Figure 5, an absorption peak with weak intensity is identified at 2,230 cm⁻¹ in all the samples' structures, corresponding to the stretching vibration of –CN of PEN [42,44]. Stronger absorption peaks are present at 1,457 and 1,576 cm⁻¹, corresponding to vibrations of the inner backbone of the PEN, while a prominent absorption peak observed at approximately 1,206 cm⁻¹ can be attributed to the stretching vibration of the aryl ether bond (Ar–O–Ar) present in the backbone structure [44]. With the exception of $P4_{PKCF0}C3$, the other three materials show a small shoulder peak at 1,626 cm⁻¹, indicating the

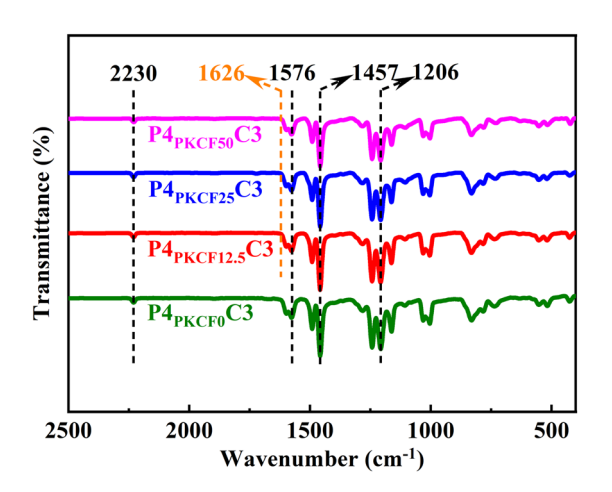


Figure 5: FTIR curves of P4_{PKCFx}C3 composite materials.

presence of both C=N stretching vibration and aromatic ring vibration overlap [55]. The presence of C=N is evidence of a Schiff base or Michell addition reaction between dopamine and KH550.

Due to the characteristics of high strength of CF, there are some difficulties in studying the microscopic morphology of PEN/PKMWCNT@Fe₃O₄/CF composites cross-section, and only the PPKCEx layer was investigated. Figure 6(a)–(d) shows SEM images of P_{PKCEx} layers at filler ratios of 0, 12.5, 25, and 50 wt%, in turn, at a scale rule of 200 µm. It is observed that the PEN films obtained using the method of non-solventogenic phase separation have finger-like pores with a pore diameter of about 20 µm, which promotes the advantage of light-weight and low-density. With the increase of filler content, the shape and diameter of the pores does not change significantly. However, the increase in filler content leads to a decrease in the compatibility of the phases within the porous membrane, and agglomeration of the PKMWCNT@Fe₃O₄ is observed inside the pores, which was particularly evident at 50 wt% addition.

Fe₃O₄ is introduced into the composite material to impart magnetic properties to the material, which facilitates the absorption of electromagnetic waves, thereby improving the electromagnetic shielding effectiveness of the material. The magnetic properties of the P_{PKCFx} layer and the P4_{PKCEx}C3 composite are tested separately. From Figure 7(a), the saturation magnetization intensity of P_{PKCEx} layer increases with the increase of magnetic filler content, and the saturation magnetization intensity of $P_{PKCF12.5}$ $P_{\rm PKCF25}$, and $P_{\rm PKCF50}$ are 3.10, 5.46, and 8.15 emu/g, respectively. Also, the trend of composites is consistent with P_{PKCFx} layer, and the M_s of $P4_{PKCF12.5}C3$, $P4_{PKCF25}C3$, and P4_{PKCF50}C3 are 0.47, 0.92, and 1.37 emu/cm³, respectively (Figure 7b). These findings suggest that incorporating PKMWCNT@Fe₃O₄ into the composites imparts magnetic properties to them. Additionally, the inclusion of a magnetic polymer layer can enhance magnetic loss, leading to improved electromagnetic shielding effectiveness. This contributes to the development of an absorption-based shielding mechanism, which effectively reduces secondary electromagnetic pollution.

The conductivity of the four composites are presented in Figure 7(c). When the PEN matrix resin is not introduced in the modified carbon nanotubes, the composite exhibits a conductivity of 1.10 S/cm. Compared with the pure PEN matrix resin, this increase in electrical conductivity is mainly attributed to the asymmetric conductive network built by the CF in the composite, which leads to a significant improvement in electrical properties. When the functionalized carbon nanotubes are introduced, the PEN layer also forms a corresponding conductive network and

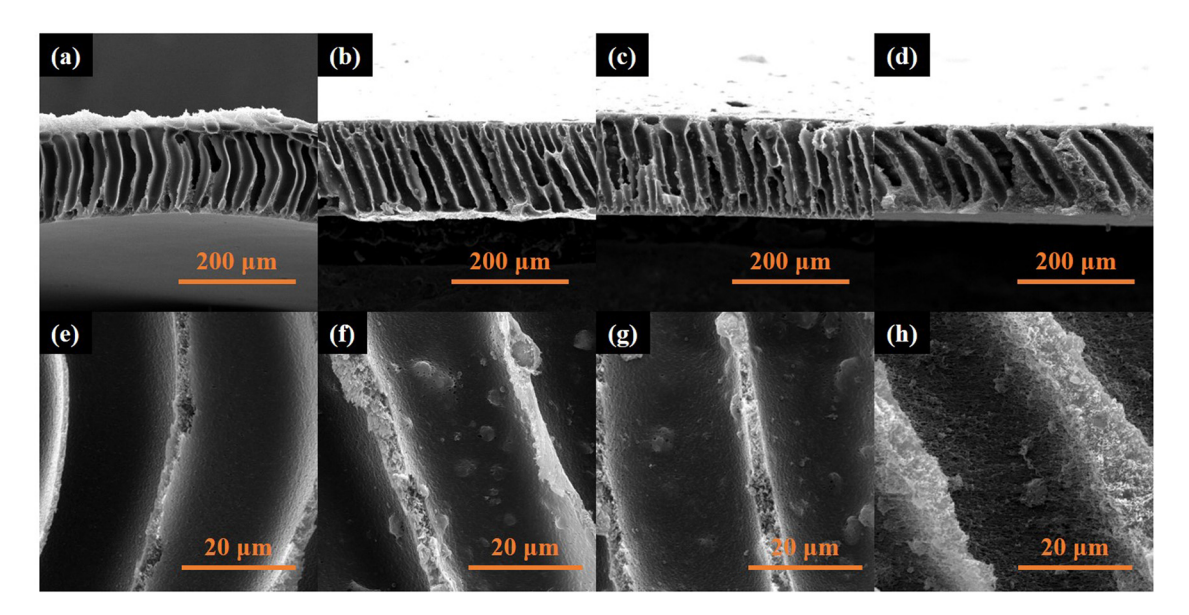


Figure 6: The SEM images of the P_{PKCF3}. (a) P_{PKCF9}.; (b) P_{PKCF12.5}; (c) P_{PKCF25}; (d) P_{PKCF50}.; (e) P_{PKCF0}.; (f) P_{PKCF12.5}; (g) P_{PKCF25}.; (h) P_{PKCF50}.

the electrical properties of the composites are further improved. With the increase of the conductive filler content, P4_{PKCF12.5}C3, P4_{PKCF25}C3, and P4_{PKCF50}C3 exhibit a gradual increase of electrical conductivity. The conductivity

values are 1.44, 1.67 and 1.90 S/cm, respectively. This result highlights a significant positive correlation between the electrical conductivity of the composites and the amount of conductive filler doping, which is closely linked to the

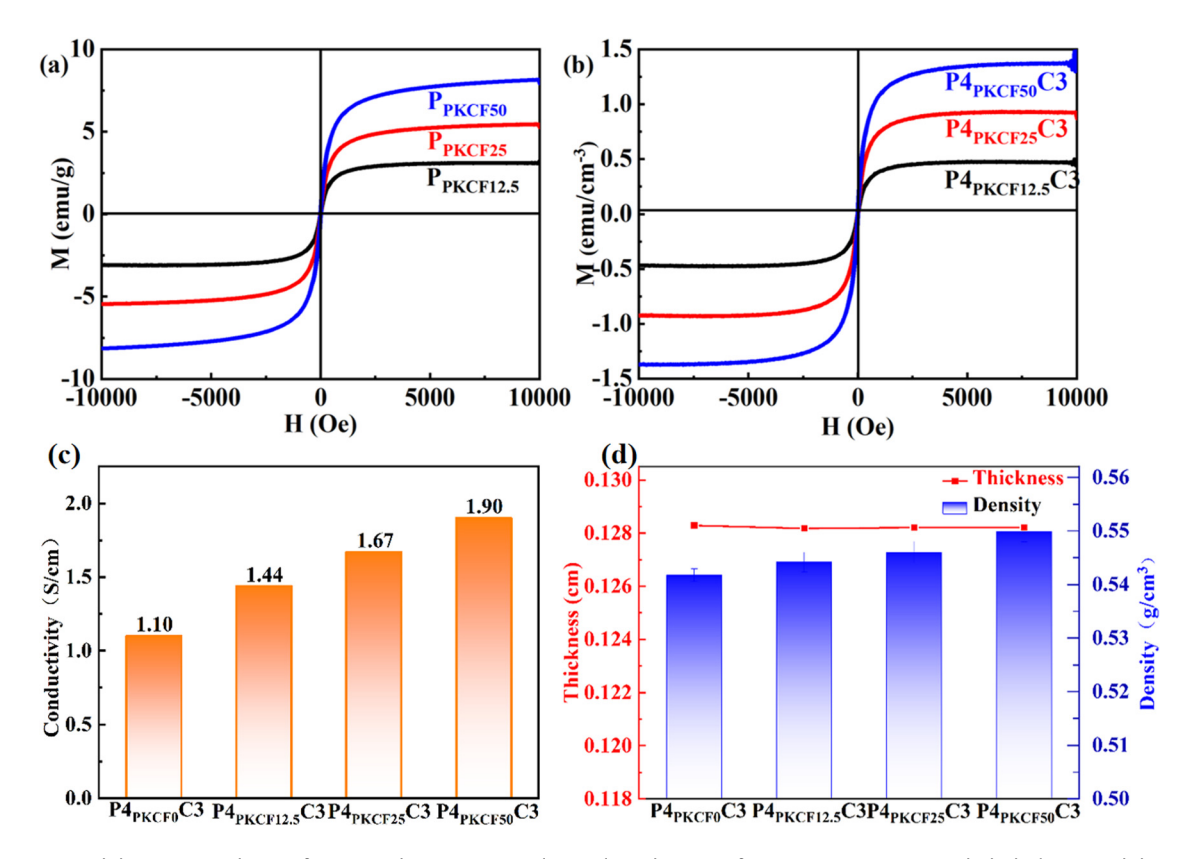


Figure 7: (a) and (b) Hysteresis loops of P_{PKCFx} and $P4_{PKCFx}C3$, (c) electrical conductivity of $P4_{PLCFx}C3$ composite, and (d) thickness and density of $P4_{PkCFx}C3$ composites.

excellent electrical conductivity of PKMWCNT@Fe₃O₄. The increased presence of PKMWCNT@Fe₃O₄ in the material leads to a higher interconnection of conductive particles within the matrix, further improving the electrical conductivity network and resulting in a gradual increase in electrical conductivity [56]. The increase in conductivity of the composite material contributes to more dielectric loss of electromagnetic waves in the interior, which is crucial for the large improvement of shielding performance.

From Figure 7(d), the thicknesses of $P4_{PKCF0}C3$, $P4_{PKCF12.5}C3$, $P4_{PKCF25}C3$, and $P4_{PKCF50}C3$ are all around 0.128 cm with negligible variations, which is consistent with the SEM results above: the pore size and thickness of the PEN layer are not significantly related to the filler content, which again proves that the material prepared by this method has a high macroscopic morphology. Meanwhile, the density of these samples slightly increases to 0.542, 0.544, 0.546, and 0.550 g/cm³, respectively. This indicates that a lightweight composite material was successfully prepared.

The electromagnetic shielding effectiveness is determined by the frequency of electromagnetic waves and the electromagnetic properties of the shielding material. Therefore, studying the effect of filler content on the electromagnetic shielding performance of composites is crucial. Figure 8(a)–(c) shows the SE_T , SE_R , and SE_A curves for the four materials, respectively. It is clear that except for $P4_{PKCF0}C3$, the EMI SE_T (Figure 8a) of the other three materials remains basically stable throughout the X-band

without any significant fluctuation. The maximum SE_T of P4_{PKCF0}C3 in this X-band is 18.5 dB, which is a great improvement in shielding efficiency compared with the almost completely wave-transparent pure PEN film, which is the result of the introduction of carbon fabric into the substrate. Besides, the content of PKMWCNT@Fe₃O₄ is an important factor in determining its electromagnetic shielding performance. With the increase in nanoparticles, the shielding effectiveness of the material also increases. The SE_T values of P4_{PKCF12.5}C3, P4_{PKCF25}C3, and P4_{PKCF50}C3 in this band are up to 34.04, 42.56, and 47.08 dB, respectively, which fully meet the requirements of commercial shielding materials. It can be attributed to the enhancement of electrical and magnetic properties caused by the addition of this double loss type of filler, resulting in more conductive losses within the material to dissipate the electromagnetic waves. Figure 8(b) shows that although the SE_T of $P4_{PKCF0}$ is the lowest, its SE_R is not lower than the other three materials, and is even higher than the other three materials when the frequency is higher than 10.5 GHz. The changes of SE_A values of the four materials (Figure 8c) are consistent with the trends of SE_T values. The highest SE_A value of $P4_{PKCF50}C3$ is 45.54 dB, and the SE_R value at the corresponding frequency is only

The SE_A/SE_T , A(eff), and the percentage values of A and R coefficients are calculated to further investigate the electromagnetic screening mechanism. Figure 8(d) displays that the SE_A/SE_T ratio of composites increased with the

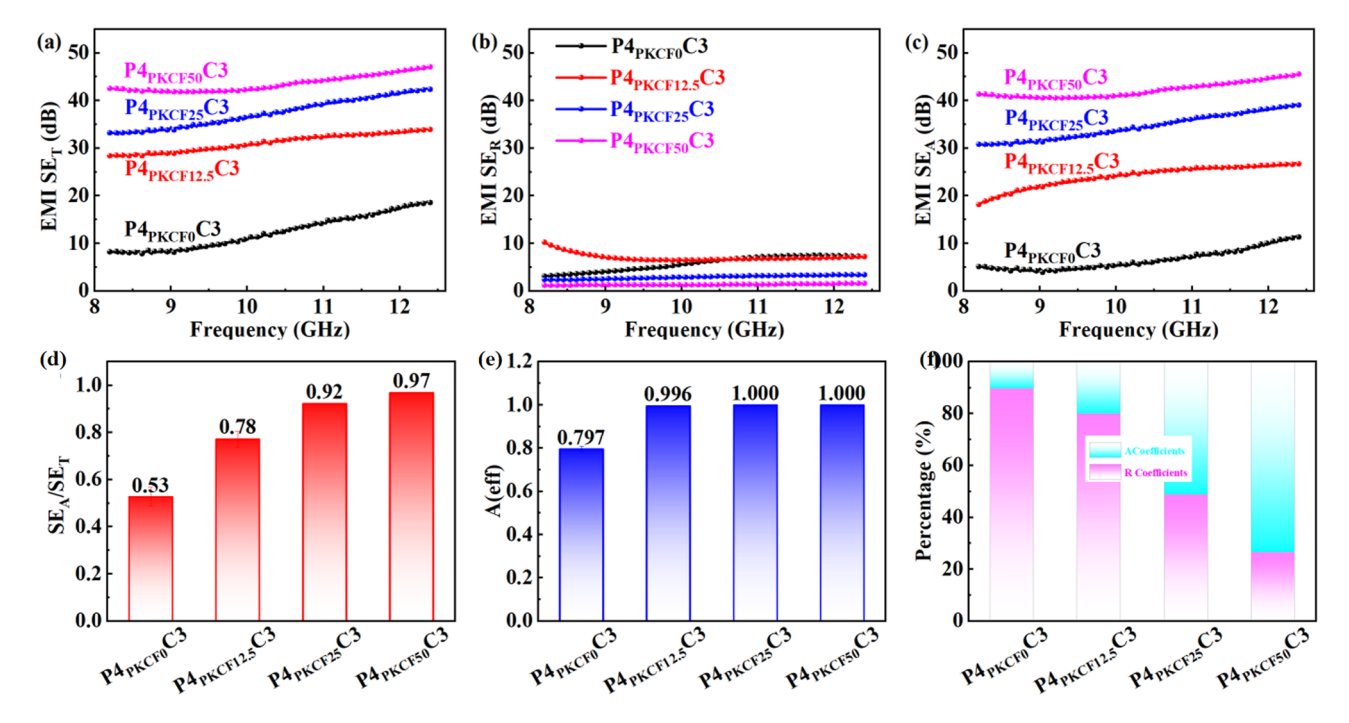


Figure 8: EMI SE data of P4_{PKCFx}C3 composites: (a) SE₇, (b) SE₈, (c) SE_A, (d) SE_A/SE_R, (e) A(eff), and (f) A, R coefficient percentage.

content of PKMWCNT@Fe₃O₄ hybrid materials increasing and values of P4_{PKCF0}C3, P4_{PKCF12.5}C3, P4_{PKCF25}C3, and P4_{PKCF50}C3 are 0.53, 0.78, 0.92, and 0.97, respectively, which represents that the introduction of magnetoelectric dual-loss nanoparticles helps to enhance the overall performance of the material and strengthen the interaction with the incident waves, thus facilitating the absorption of electromagnetic waves inside the material and improving the absorption efficiency to reduce the secondary pollution of electromagnetic waves. Meanwhile, the results of A(eff) also show that the increase in filler content increases the absorption and shielding efficiency of the materials (Figure 8e). The A(eff) of the four materials is 0.797, 0.996. 1.000, and 1.000, respectively. It means that when A(eff) is close to 1 the content of PKMWCNT@Fe3O4 in the PEN layer is 25 wt%. This is a reflection of the high absorption efficiency of this type of shielding material. In addition, the large A and R percent ratios calculated results are recorded in Figure 8(f). It shows that the influence of filler content on the shielding effect is also well illustrated by the A and R ratios calculated, where the material A-factor percentage increases and the R-factor percentage decreases with the increasing content of PKMWCNT@Fe₃O₄. When the filler content is 50 wt%, the A/Rratio of the material is 73/27. This reveals the difference between the reflective and absorptive efficiency of the material and proves its absorption-driven shielding mechanism in P4_{PKCF50}C3 sample.

To sum up, the above data indicate that the electromagnetic shielding effectiveness can be effectively adjusted by the content of this magnetoelectric dual-loss PKMWCNT@Fe₃O₄ nanoparticle. Also, the conductivity as well as magnetic properties of the material are improved due to the increase of fillers. This is mainly due to the conductive losses caused by the interaction of a large number of free electrons in the matrix with electromagnetic waves, while eddy current losses due to the magnetic properties of this type of carbon nanotubes can also enhance the shielding effectiveness of the material. Specifically, a large number of free electrons within the composites form electrical energy under the action of incident electromagnetic waves, which is then converted into thermal energy. Second, due to the in situ growth of Fe₃O₄ particles on the carbon nanotubes, very small interfaces are formed between them. The introduction of Fe₃O₄ particles into PEN layer causes the formation of more interfaces in the porous layer, which helps to enhance the interfacial polarization and thus energy dissipation.

Figure 9 shows the trend of electrical conductivity, saturation magnetization strength, and shielding effectiveness of $P4_{PKCFx}C3$ composite materials. It can be seen that EMI SE increases continuously with the increase of conductivity. This change is mainly due to the presence of a large number of free electrons in the material that interact

with electromagnetic waves and dissipate the electromagnetic waves. The EMI SE of the composite also increases with its saturation magnetization strength. The variation trend shows a certain correlation with the saturation magnetization intensity. The results indicate that the hybridized PKMWCNT@Fe₃O₄ plays an important role in enhancing both conductivity and magnetism, proving that it is a double-loss type of filler, which contributes to the improvement of electromagnetic shielding performance in the composites. In this work, the porous morphology of the PEN layer, the electrical conductivity of the CF cloth, and the dual-loss property of the filler make the material reflect and absorb the electromagnetic wave many times, so that the material has superior electromagnetic shielding performance. The introduction of magnetic fillers allows the material to have a high shielding effectiveness even at low conductivity value.

Based on the provided information, the mechanism of the material can be summarized as shown in Figure 10. The PEN and CF layers have distinct roles in the process. Electromagnetic waves are dissipated within the PEN magnetic layer through hysteresis loss, eddy current loss, and interface polarization [57,58]. Between the CF layers, the dissipation of electromagnetic waves mainly occurs through conductive losses and interfacial polarization. In addition, the unique structure of the material contributes to enhanced shielding effectiveness in several ways. The magnetic PEN layer's dielectric constant near the air allows electromagnetic waves to smoothly enter the material and be effectively consumed. Additionally, the porous structure of the PEN layer generates interfacial polarization, which further aids in dissipating electromagnetic waves. Furthermore, the impedance mismatches within the alternating multilayers of PEN and CF lead to multiple reflections of electromagnetic waves [59]. As a result, the PEN layer experiences hysteresis and eddy current losses, while the CF layer

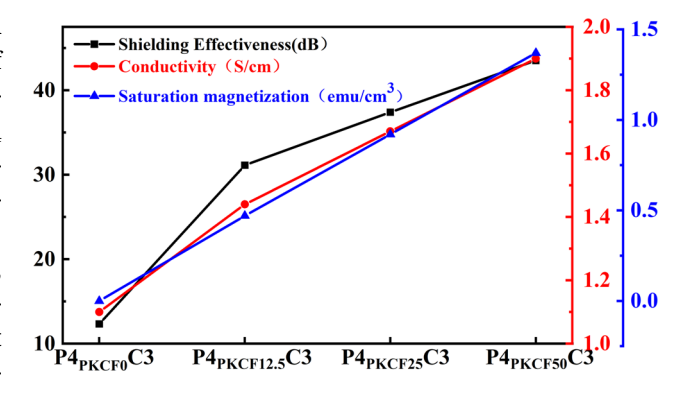


Figure 9: Trend of electrical conductivity, saturation magnetization strength, and shielding effectiveness of P4_{PKCFx}C3 composite materials.

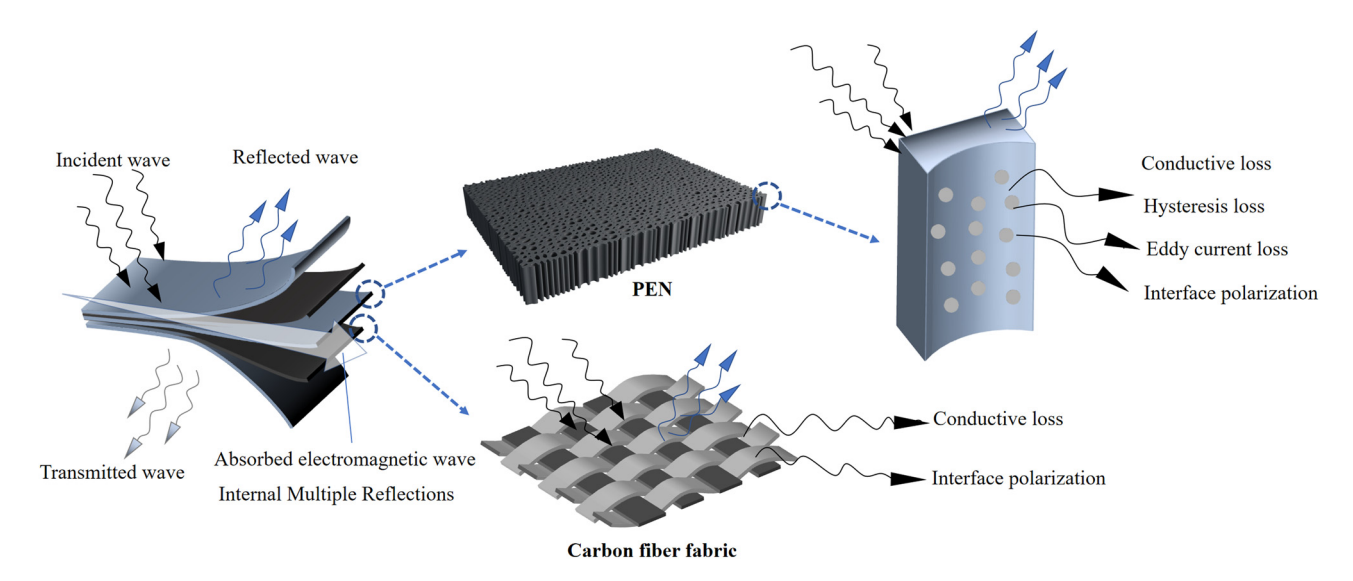


Figure 10: Diagram of the electromagnetic shielding mechanism of P4_{PKCFx}C3 composite materials.

incurs conductive losses. These characteristics enable the composites to effectively follow an absorption-based shielding mechanism.

Figure 11 shows the calculated SSE/t values for the P4_{PKCFx}C3 composites. This value increases with filler content increasing, and the SSE/t values for P4_{PKCF0}C3, P4_{PKCF12.5}C3, P4_{PKCF30}C3 are 177, 446, 534, and 617 dB cm² g⁻¹, respectively. It is clear that these composites have lower density and better SSE/t.

Table 1 presents key parameters of the $P4_{PKCFx}C3$ composite. Results confirm that the composite has a stable thickness with the advantages of low density and high efficiency. This favorable performance can be primarily attributed to the ideal combination of the multilayer and porous structure of the PEN and the magnetoelectric doubleloss type filler. Furthermore, the utilization of low-cost CF fabric as the conductive framework not only meets the

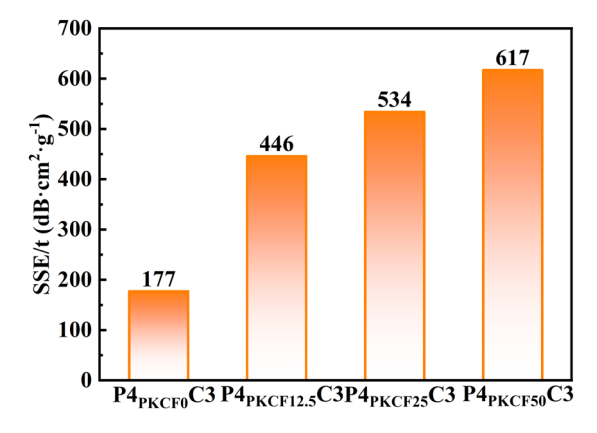


Figure 11: SSE/t data of P4_{PKCFx}C3 composite materials.

standards set by the commercial industry but also offers excellent cost-effectiveness. This is in contrast to carbon/polymer composites prepared with alternative fillers like monolayer graphene, which tend to be more expensive.

To be practical, composite materials also need to have excellent mechanical strength. The mechanical strength of the material directly affects the life and reliability of the material. Table 2 lists the mechanical properties of P4_{PKCEx}C3 varied as a function of filler content. Specifically, the tensile strength of P4_{PKCF0}C3 is 42.54 MPa, which is 3,198% higher than that of the pure porous PEN film [60]. In addition, as the PKMWCNT@Fe₃O₄ content gradually increases from 12.5 to 50 wt%, the composites exhibit tensile strengths of 46.62, 44.57, and 43.98 MPa, respectively. This is the advantage of the good inherent properties of the CF. When the porous PEN structure is damaged during stretching, the interwoven strong CF are not affected and the composite can be further stretched until the interwoven structure of the CF is broken. Even if the original interwoven structure is destroyed, the composite still can be extended, so the material shows a large elongation at break. Take for instances, the elongation

Table 1: Critical data of P4_{PKCFx}C3 composite materials

Sample	Thickness (mm)	Density (g/cm³)	EMI- SE (dB)	SSE/ <i>t</i> (dB cm ² g ⁻¹)
P4 _{PKCF0} C3	1.283	0.542	12	177
P4 _{PKCF12.5} C3	1.282	0.544	31	446
P4 _{PKCF25} C3	1.282	0.546	37	534
P4 _{PKCF50} C3	1.282	0.550	44	617

Table 2: Critical mechanical data of P4_{PKCFx}C3 composite materials

Sample	Elongation at break (%)	Tensile strength (MPa)	Tensile modulus (GPa)
P4 _{PKCF0} C3	44.82	42.54	4.778
P4 _{PKCF12.5} C3	46.62	46.62	4.869
P4 _{PKCF25} C3	44.57	44.57	4.687
P4 _{PKCF50} C3	43.32	43.98	4.749

at break of P4_{PKCF12.5}C3 is as high as 46.62%. Therefore, the inclusion of CF not only imparts high mechanical strength to the composite but also greatly improves its toughness.

4 Conclusion

This work studied the effect of magnetoelectric double-loss PKMWCNT@Fe₃O₄ and CF on the electromagnetic shielding performance of PEN composites. The homogeneous distribution of PKMWCNT@Fe3O4 within the PEN phase, combined with the alternating multilayer structure formed by CF, effectively creates a continuous conductive network. As a result, the material exhibits high conductivity (1.90 S/cm) and good saturation magnetization strength ($M_s = 1.37 \text{ emu/cm}^3$), synergistically enhancing the shielding effectiveness with a high SE_T value of 47.08 dB. Furthermore, the SE_A/SE_T is 97%, indicating that the material predominantly follows an absorption-dominated shielding mechanism. At the same time, the use of NIPs imparts a porous structure to PEN layer in the material, significantly reducing the density of the material down to 0.54 g/cm³. Even with the addition of high content of PKMWCNT@Fe₃O₄, the functional PEN composites maintain high mechanical properties. Therefore, this lightweight and high-performance PEN composite material is anticipated to find extensive applications in the electromagnetic shielding field.

Funding information: This project was supported by the National Natural Science Foundation of China (Grant no. 52073039).

Author contributions: All authors have accepted responsibility for the entire content of this manuscript and approved its submission.

Conflict of interest: The authors state no conflict of interest.

References

- Liu C, Wang L, Liu S, Tong L, Liu X. Fabrication strategies of polymer-based electromagnetic interference shielding materials. Adv Ind Eng Polym Res. 2020;3(4):149-59.
- Liu M, Chen K, Shi Y, Wang H, Wu S, Huang R, et al. High-performance flexible nanocomposites with superior fire safety and ultraefficient electromagnetic interference shielding. J Mater Sci Technol. 2023;166:133-44.
- Huang D, Chen Y, Zhang Li, Sheng X. Flexible thermoregulatory microcapsule/polyurethane-MXene composite films with multiple thermal management functionalities and excellent EMI shielding performance. J Mater Sci Technol. 2023;165:27-38.
- [4] Maestre CVV, Santos GN. Effect of bismuth oxide nanoparticle on the electromagnetic interference shielding and thermal stability of industrial waste based-geopolymer composites. Sci Rep. 2023;13(1):1787.
- [5] Zhao B, Hamidinejad M, Wang S, Bai P, Che R, Zhang R, et al. Advances in electromagnetic shielding properties of composite foams. J Mater Chem A. 2021;9(14):8896-949.
- Cheng J, Li C, Xiong Y, Zhang H, Raza H, Ullah S, et al. Recent advances in design strategies and multifunctionality of flexible electromagnetic interference shielding materials. Nano-Micro Lett. 2022:14(1):80.
- Li J, Zhang S, Wang L, Liu X. In situ growth of Fe₃O₄ nanoparticles in poly(arylene ether nitrile)/graphene/carbon nanotube foams for electromagnetic interference shielding. ACS Appl Nano Mater. 2023;6(9):7802-13.
- Deng Y, Han X, Chen H, Zhao C, Chen Y, Zhou J, et al. Regulating the electrical and mechanical properties of TaS2 films via van der Waals and electrostatic interaction for high performance electromagnetic interference shielding. Nano-Micro Lett. 2023;15(1):106.
- Maruthi N, Faisal M, Raghavendra N. Conducting polymer based composites as efficient EMI shielding materials: a comprehensive review and future prospects. Synth Met. 2021;272:116664.
- Yao Y, Jin S, Zou H, Li L, Ma X, Lv G, et al. Polymer-based lightweight materials for electromagnetic interference shielding: a review. J Mater Sci. 2021;56(11):6549-80.
- [11] Liang J, Bai M, Gu Y, Wang S, Li M, Zhang Z. Enhanced electromagnetic shielding property and anisotropic shielding behavior of corrugated carbon fiber felt composite and its sandwich structure. Compos Part A-Appl Sci Manuf. 2021;149:106481.
- Kruželák J, Kvasničáková A, Hložeková K, Hudec I. Progress in Γ121 polymers and polymer composites used as efficient materials for EMI shielding. Nanoscale Adv. 2021;3(1):123-72.
- Wanasinghe D, Aslani F. A review on recent advancement of electromagnetic interference shielding novel metallic materials and processes. Compos Part B-Eng. 2019;176:107207.
- [14] Ayub S, Guan BH, Ahmad F, Oluwatobi YA, Nisa ZU, Javed MF, et al. Graphene and iron reinforced polymer composite electromagnetic shielding applications: a review. Polymers. 2021;13(15):2580.
- Tiwari A, Tiwari A, Bhatia A, Chadha U, Kandregula S, Selvaraj SK, et al. Nanomaterials for electromagnetic interference shielding applications: a review. Nano. 2022;17(2):2230001.
- Lee H, Ryu SH, Kwon SJ, Choi JR, Lee S, Park B. Absorption-dominant mmWave EMI shielding films with ultralow reflection using

- ferromagnetic resonance frequency tunable M-type ferrites. Nano-Micro Lett. 2023;15(1):76.
- [17] Xue T, Yang Y, Yu D, Wali Q, Wang Z, Cao X, et al. 3D printed integrated gradient-conductive MXene/CNT/polyimide aerogel frames for electromagnetic interference shielding with ultra-low reflection. Nano-Micro Lett. 2023;15(1):45.
- [18] Wei Z, Cai Y, Xie Z, Meng Y, Zhan Y, Hu X, et al. Green electromagnetic interference shielding films with unique and interconnected 3D magnetic/conductive interfaces. Appl Surf Sci. 2023;636:157841.
- [19] Wang M, Tian L, Zhang Q, You X, Yang J, Dong S. Absorption-based electromagnetic interference shielding composites with sandwich structure by one-step electrodeposition method. Carbon. 2023:202:414-24
- [20] Zhou M, Tan S, Wang J, Wu Y, Liang L, Ji G. "Three-in-One" multiscale structural design of carbon fiber-based composites for personal electromagnetic protection and thermal management. Nano-Micro Lett. 2023;15(1):176.
- [21] Qian K, Zhou J, Miao M, Wu H, Thaiboonrod S, Fang J, et al. Highly ordered thermoplastic polyurethane/aramid nanofiber conductive foams modulated by Kevlar polyanion for piezoresistive sensing and electromagnetic interference shielding. Nano-Micro Lett. 2023;15(1):88.
- [22] Wang C, Li J, Guo S. High-performance electromagnetic wave absorption by designing the multilayer graphene/thermoplastic polyurethane porous composites with gradient foam ratio structure. Compos Part A-Appl Sci Manuf. 2019;125:105522.
- [23] Kumar R, Sahoo S, Joanni E, Singh RK, Tan WK, Kar KK, et al. Recent progress on carbon-based composite materials for microwave electromagnetic interference shielding. Carbon. 2021;177:304-31.
- [24] Xia Y, Gao W, Gao C. A review on graphene-based electromagnetic functional materials: electromagnetic wave shielding and absorption. Adv Funct Mater. 2022;32(42):2204591.
- [25] Igbal A, Sambyal P, Koo CM. 2D MXenes for electromagnetic shielding: a review. Adv Funct Mater. 2020;30(47):2000883.
- [26] Ran L, Qiu L, Sun F, Chen Z, Zhao L, Yi L, et al. Multilayer assembly of strong and tough MXene/cellulose films for excellent electromagnetic shielding. J Alloy Compd. 2023;961:171020.
- [27] Zhang Y, Ruan K, Gu J. Flexible sandwich-structured electromagnetic interference shielding nanocomposite films with excellent thermal conductivities. Small. 2021;17(42):2101951.
- [28] Wang Y, Peng HK, Li TT, Shiu BC, Ren HT, Zhang X, et al. MXenecoated conductive composite film with ultrathin, flexible, selfcleaning for high-performance electromagnetic interference shielding. Chem Eng J. 2021;412:128681.
- [29] Zhu H, Fu K, Yang B, Li Y. Nickel-coated nylon sandwich film for combination of lightning strike protection and electromagnetic interference shielding of CFRP composite. Compos Sci Technol. 2021:207:108675.
- [30] Lv M, Liu H, He L, Zheng B, Tan Q, Hassan M, et al. Absorptiondominated electromagnetic interference shielding assembled composites based on modular design with infrared camouflage and response switching. Compos Sci Technol. 2023;231:116218.
- [31] Wang H, Li S, Liu M, Li J, Zhou X. Review on shielding mechanism and structural design of electromagnetic interference shielding composites. Macromol Mater Eng. 2021;306(6):2100032.
- [32] Wanasinghe D, Aslani F, Ma G, Habibi D. Advancements in electromagnetic interference shielding cementitious composites. Constr Build Mater. 2020;231:117116.
- [33] Srivastava SK, Manna K, Recent advancements in the electromagnetic interference shielding performance of nanostructured

- materials and their nanocomposites: a review. J Mater Chem A. 2022:10(14):7431-96.
- [34] Abbasi H, Antunes M, Ignacio Velasco J. Recent advances in carbonbased polymer nanocomposites for electromagnetic interference shielding. Prog Mater Sci. 2019;103:319-73.
- [35] Jiang D, Murugadoss V, Wang Y, Lin J, Ding T, Wang Z, et al. Electromagnetic interference shielding polymers and nanocomposites - a review. Polym Rev. 2019;59(2):280-337.
- [36] Liu S, Qin S, Jiang Y, Song P, Wang H. Lightweight high-performance carbon-polymer nanocomposites for electromagnetic interference shielding. Compos Part A-Appl Sci Manuf. 2021;145:106376.
- [37] Jia Z, Zhang M, Liu B, Wang F, Wei G, Su Z. Graphene foams for electromagnetic interference shielding: a review. ACS Appl Nano Mater. 2020;3(7):6140-55.
- [38] Kong D, Li J, Guo A, Xiao X. High temperature electromagnetic shielding shape memory polymer composite. Chem Eng J. 2021;408:127365.
- [39] Zhang Y, Ma Z, Ruan K, Gu J. Flexible Ti₃C2T_x/(Aramid Nanonber/ PVA) composite films for superior electromagnetic interference shielding. Research. 2022;2022:9780290.
- [40] Zheng X, Zhang H, Jiang R, Liu Z, Zhu S, Li W, et al. Lightweight polyurethane composite foam for electromagnetic interference shielding with high absorption characteristic. J Colloid Interface Sci. 2023;649:279-89.
- [41] Li T, Lin G, He L, Xia Y, Xu X, Liu Y, et al. Structural design and properties of crystalline polyarylene ether nitrile copolymer. Colloids Surf A-Physicochem Eng Asp. 2023;659:130788.
- [42] He L, Lin G, Liu X, Tong L. Polyarylene ether nitrile composites film with self-reinforcing effect by cross-linking and crystallization synergy. Polymer. 2022;262:125457.
- [43] Chu S, Liu C, Feng X, Wu H, Liu X. Aromatic polymer dual-confined magnetic metal-organic framework microspheres enable highly efficient removal of dyes, heavy metals, and antibiotics. Chem Eng J. 2023;472:145159.
- [44] He L, Tong L, Bai Z, Lin G, Xia Y, Liu X. Investigation of the controllable thermal curing reaction for ultrahigh T-g polyarylene ether nitrile compositions. Polymer. 2022;254:125064.
- [45] He L, Tong L, Xia Y, Lin G, Wang T, Zhang W, et al. Advanced composites based on end-capped polyarylene ether nitrile/ bisphthalonitrile with controllable thermal curing reaction. Polymer. 2022;245:124695.
- [46] Liu S, Liu C, Bai Z, Lin G, Liu X. Metal-organic frameworks mediated interface engineering of polymer nanocomposites for enhanced dielectric constant and low dielectric loss. Surf Interfaces. 2023;36:102586.
- [47] Wang P, Wang M, Song T, Chen J, Liu X, et al. Anti-bacterial robust Ag@PDA/PEN electrospinning nanofibrous membrane for oil-water separation. J Water Process Eng. 2023;51:103358.
- [48] He L, Zhang W, Liu X, Tong L. Substantial improvement of thermal conductivity and mechanical properties of polymer composites by incorporation of boron nitride nanosheets and modulation of thermal curing reaction. Polym Compos. 2023. doi: 10.1002/pc. 27915.
- [49] Wu N, Hu Q, Wei R, Mai X, Naik N, Pan D, et al. Review on the electromagnetic interference shielding properties of carbon based materials and their novel composites: recent progress, challenges and prospects. Carbon. 2021;176:88-105.
- [50] Zhang L-Q, Yang B, Teng J, Lei J, Yan DX, Zhong GJ, et al. Tunable electromagnetic interference shielding effectiveness multilayer

DE GRUYTER

- assembly of regenerated cellulose as a supporting substrate and carbon nanotubes/polymer as a functional layer. J Mater Chem C. 2017;5(12):3130-8.
- [51] Wu Z, Xu Y, Zhang X, Shen G, Yu R. Microwave plasma treated carbon nanotubes and their electrochemical biosensing application. Talanta. 2007;72(4):1336-41.
- [52] Parreira LS, Silva JCM, Simões FR, Cordeiro MAL, Sato RH, Leite ER, et al. PtSn electrocatalyst supported on MWCNT-COOH: investigating the ethanol oxidation reaction. Chemelectrochem. 2017;4(8):1950-8.
- [53] Wan D, Wang G, Li W, Wei X. Investigation into the morphology and structure of magnetic bentonite nanocomposites with their catalytic activity. Appl Surf Sci. 2017;413:398-407.
- [54] Wan X, Zhan Y, Long Z, Zeng G, Ren Y, He Y. High-performance magnetic poly (arylene ether nitrile) nanocomposites: comodification of Fe₃O₄ via mussel inspired poly(dopamine) and amino functionalized silane KH550. Appl Surf Sci. 2017;425:905-14.
- [55] Wan X, Zhan Y, Long Z, Zeng G, He Y. Core@double-shell structured magnetic halloysite nanotube nano-hybrid as efficient recyclable

- adsorbent for methylene blue removal. Chem Eng J. 2017:330:491-504.
- [56] Liu C, Feng X, Liu S, Lin G, Bai Z, Wang L, et al. Graphene reinforced nanoarchitectonics of 3D interconnected magnetic-dielectric frameworks for high-efficient and anti-corrosive microwave absorbers. J Mater Sci Technol. 2024;168:194-207.
- Liu C, Liu S, Feng X, Zhu K, Lin G, Bai Z, et al. Phthalocyaninemediated interfacial self-assembly of magnetic graphene nanocomposites toward low-frequency electromagnetic wave absorption. Chem Eng J. 2023;452:139483.
- [58] Liu C, Liu S, Zhu K, Feng X, Bai Z, Lin G, et al. Straightforward modulation of graphene nanosheets with magnetic nanoclusters for ultrathin microwave absorption materials. Appl Surf Sci. 2023;607:154998.
- [59] Wu H, Liu C, Chu S, Feng X, Liu X. Integrated super-engineering polymeric electromagnetic interference shielding films withstanding the extreme environments. Chem Eng J. 2023;472:144853.
- [60] Tang X, Lin G, Liu C, Cao T, Xia Y, Yi K, et al. Lightweight and tough multilayered composite based on poly(aryl ether nitrile)/carbon fiber cloth for electromagnetic interference shielding. Colloids Surf A-Physicochem Eng Asp. 2022;650:129578.